Received: 10 January 2023 | Revised: 3 May 2023 | Accepted: 12 May 2023

DOI: 10.1002/elan.202300013

RESEARCH ARTICLE

ELECTROANALYSIS

A novel strategy for fabrication, activation and cleaning of fully 3D printed flexible planar electrochemical platforms

Cristian Grazioli | **Rossella Svigelj** | **Nicolò Dossi**

Department of Agrifood, Environmental and Animal Science, University of Udine, Udine, Italy

Correspondence
Nicolò Dossi, Department of Agrifood, Environmental and Animal Science, University of Udine, via Cotonificio 108, 33100, Udine, Italy.
Email: nicolo.dossi@uniud.it

Abstract

In recent years, 3D printing of carbon-based conductive filaments has received growing attention for assembling electrodes to be used in a wide variety of electroanalytical devices and applications. Despite the large amount of work present in literature concerning the development of three-dimensional (3D) conductive structures, its potential as dry deposition method for assembling two-dimensional (2D) electrodes to be used in planar configuration is still largely unexplored. In fact, the possibility to rapidly change the geometry of the electrochemical circuits, associated with the reduction of waste and the absence of solvents, which are instead important components of ink and paste formulations, makes this strategy a valid green and efficient alternative to other deposition approaches such as screen-printing technology. We report here a rapid and solvent-free method for assembling fully 3D printed flexible planar electroanalytical platforms (3DEPs) to be used with microliters of liquid. At the same time, a novel protocol for the surface pre-treatment of 3D printed electrodes based on ultrasonication in aqueous NaOH solution followed by electrochemical activation using the same medium, is presented. In addition, the same procedure has proved to be efficient for cleaning the electrode surface after electrochemical passivation, thus confirming the validity of both time-efficient and environmentally-friendly assembling and activation/cleaning procedures developed which allow efficient and reusable electrodes to be produced. Finally, 3DEPs were tested by a proof-of-concept quantification of a commonly used food dye (Brilliant Blue, E-133) in commercial solutions used for homemade food coloring.

KEYWORDS

3D printed electrodes, conductive filaments, electrochemical sensors, electrode surface activation, low-cost analytical devices, ultrasonic cleaning

1 | INTRODUCTION

3D printing technologies are nowadays widely available and used for a lot of applications, ranging from building objects for everyday life to development of prototypes for medical applications [1–3]. In this context, among the different 3D printing technologies available, fused deposition modeling (FDM), due to its advantages such as

low fabrication costs, time efficiency and versatility, has received great interest also in the field of analytical chemistry for assembling custom labware and components [4–6]. More recently, in addition to conventional thermoplastic materials used for printing, such as polylactic acid (PLA) or acrylonitrile butadiene styrene (ABS), new biocompatible and biodegradable materials, such as polycaprolactone (PCL), have found extensive use not only for biomedical purposes but also for analytical applications [7–10].

Moreover, conductive filaments containing carbon black, carbon nanomaterials and graphene as additives have been recently developed and put on the market [11–14]. They have been used to develop not only conductive tracks for simple electrical circuits but also electrodes to be used, as printed or with further modification, for electrochemical purposes [15–22].

In particular, different types of electrode geometries have been developed in recent years, from multilayer rod-like to thin-film electrodes [23–27]. In some cases, 3D printed conductive tracks and electrodes have been incorporated in a bulk of non-conductive material such as PLA or ABS by means of 3D printing machines equipped with double extruder to obtain fully integrated planar devices [28–30].

It is worth noting that, prior to their use for electrochemical sensing, 3D printed electrodes must be activated in order to eliminate as much as possible the insulating thermoplastic component and expose the conductive portion to the outside. To this aim, a lot of different activation procedures are described in literature such as thermal procedures, exploiting temperature for thermal annealing, solvent-based methods, adopted for dissolving the polymeric matrix and electrochemical procedures, applying a potential difference to electrodes. These methodologies have been used either individually or in combination as well as sequentially and often coupled with mechanical polishing. Their benefits and drawbacks have been thoroughly documented in the literature [14, 23, 25, 31–38].

In this article, an easy procedure for assembling fully 3D printed flexible electroanalytical platforms (3DEPs) with shape and functionality comparable to screen printed electrodes and designed to work also in planar configuration with few microliters of sample, is presented. To this aim, two polyester-based filaments (PLA/graphene and PCL filaments) which are supposed to have good chemical compatibility and adhesion [39], were used to assemble a single monobloc integrating the electrochemical circuit.

The electrode manufacturing process made possible the fabrication of multi-material planar electrochemical cells characterized by a perfectly smooth surface with no discontinuity and irregularities using a simple 3D printer equipped with a single extruder. The procedure, carried out in two steps, allowed conductive circuits (conductive PLA) and insulating supports (PCL sheets) to be printed separately and to be integrated at a later time, thus avoiding the change of the filament during the printing phase and reducing the waste of material. The use of vacuum oven ensured the complete elimination of any air bubbles present in the PCL when the two material were incorporated.

The proposed assembling approach was accompanied by a novel activation procedure, based on the use of sonication in aqueous NaOH solution, adopted in the past mainly for post-processing and cleaning of 3D printed objects and never exploited before for improving the performance of 3D printed conductive elements. In fact, sonication in basic environment, carried out after the printing process and just before the electrochemical activation, promoted the hydrolysis of both PCL and PLA [40–41], thus helping the conductive material at the electrode surface to be exposed [11, 33, 42]. This procedure of pre-treatment, unlike most others, did not require sophisticated technologies, organic solvents or high temperature and it is quite fast. To optimize the procedure, sonication (SA) and electrochemical activation (EA), consisting of an anodic and cathodic step, were firstly evaluated separately and then coupled in sequence.

In addition, the mechanical action of ultrasound, such as streaming, microjets and shockwave combined with its capacity to accelerate the hydrolysis reactions were also profitably adopted together with electrochemical activation to clean [43, 44] and restore the electrode surface in case of passivation. Surprisingly, the procedure of pre-treatment developed allowed electrochemical activity to be easily regenerated enabling reuse of the devices for several times.

Finally, 3DEPs were tested for the proof-of-concept quantification of a commonly used food dye (Brilliant Blue, E-133) in commercial solutions used for homemade food coloring.

2 | EXPERIMENTAL

2.1 | Reagents, materials and equipment

Potassium hexacyanoferrate(II), erioglaucine (Brilliant Blue, E-133), Sunset Yellow FCF (E-110), 4-(2-hydroxyethyl)phenol (tyrosol, Ty), 4-hydroxybenzoic acid (HBA), potassium chloride, sodium phosphate monobasic dihydrate, sodium phosphate dibasic dihydrate and sodium hydroxide were purchased from Sigma-Aldrich (Milan, IT). PCL filament (Facilan™ Ortho Natural

Elogiam) and conductive graphene/PLA composite material (Black Magic 3D, New York, USA) were purchased from Filoprint (Florence, IT). Designs of both electrodes and supports were made with the Autodesk® Fusion 360 software and processed by the Ultimaker Cura slicer software. They were 3D printed using a FLSUN Cube 3D printer (FLSUN, Zhengzhou, Henan, China) provided with a removable 3 mm glass bed placed above the heating bed.

Aqueous 0.1 M KCl, 0.1 M sodium phosphate monobasic dihydrate + sodium phosphate dibasic dihydrate (pH 7) and 0.01 M H_2SO_4 + 0.1 M KCl solutions were prepared in high purity deionized water (18.2 MΩ cm) purified by a PURELAB® Flex 3 system (Elga LabWater, High Wycombe, UK) and used as supporting electrolytes in voltammetric measurements.

Stock standard solutions (10 mM) of all analytes were prepared by adding weighed amounts to known volumes of supporting electrolytes.

Electrochemical measurements were conducted with a 730E CHI potentiostat (CH Instruments, Austin, TX, USA) using an Ag/AgCl (3 M KCl) reference electrode. The morphology of printed electrodes was investigated using a ZEISS EVO 40 SEM (Zeiss Group, Jena, Germany). SEM imaging was carried out with a 20 kV electron beam using an inlens secondary electron detector at a working distance of 11 mm. Ultrasonication of 3D printed electrodes was performed using a Bransonic 1210 ultrasonic cleaner (47 kHz) acquired from Branson (Danbury, USA). Spectrophotometric measurements were performed using a Varian Cary 50 Bio UV–vis spectrophotometer in the range 400–700 nm.

2.2 | Design and assembling of 3DEPs

The geometry of 3D printed electrochemical circuits, consisting of PLA/graphene working (WE), counter (CE), and pseudo-reference (PRE) electrodes, was inspired by commercial screen-printed electrodes.

In more details, planar supports (dimensions 100 × 120 × 0.8 mm, width × depth × height) were printed by using commercially available polycaprolactone filament. They were printed on the removable 3 mm glass placed above the heating bed of the printer in order to obtain printed units with an extremely smooth side, free from imperfections due to nozzle movement. The conditions used for PCL printing were: nozzle aperture 0.4mm, printing speed 50 mm s^{-1}, print layer height 0.2mm, extrusion and bed temperature of 140 °C and 65 °C, respectively. The selected printing temperatures ensured low viscosity of PCL in order to allow fast extrusion and at the same time obtain good layer adhesion and levelling of the melt material.

PCL supports were firstly printed (Figure 1A) and set aside in order to reduce the time and waste of material due to the filament change required for subsequently printing the graphene/PLA electrochemical circuits.

Conductive tracks 0.2 mm thick to be used as WE, CE and PRE electrodes were printed onto the glass with graphene/PLA filament by using nozzle with aperture of 0.4 mm, layer height of 0.2 mm, printing speed of 20 mm s^{-1}, extrusion and bed temperature of 220 °C and 65 °C, respectively (Figure 1B). After printing a series of 24 electrochemical three-electrode circuits, but before their complete cooling down, the glass was removed from the heated bed of the printer and quickly placed in a vacuum oven, preheated at 50 °C, with the adhering conductive printed tracks facing up.

A PCL support was next sandwiched between the glass bed containing the printed electrodes and another glass plate using a weight of about 60 g to slightly compress the system. The initial temperature of 50 °C was chosen to be close enough to that set for the printing bed during PLA/graphene printing in order to avoid detachment of the electrodes from the glass. At the same time, it was lower than melting point of PCL to avoid its immediate melting. Then, after closing the oven, the air inside the chamber was evacuated to remove air bubbles trapped between PCL and PLA with the aim to reduce as much as possible imperfections in the final assembly. Subsequently, the temperature was increased to 80 °C in order to melt PCL. Phase transition of PCL was monitored by naked eye observing the change of its optical properties from opaque to transparent during phase transition. During this melting step, electrochemical circuits adhering to the glass surface were incorporated into the PCL support. Finally, the internal pressure of the vacuum oven was brought back to the ambient pressure to reduce the tiny cavities remained inside the PLC support integrating the electrodes, taking advantage from the extra pressure provided by atmosphere (Figure 1C). Upon cooling and consequent PCL solidification, the monobloc detached from the glass bed resulted to be a perfectly smooth flexible planar platform where conductive tracks were completely embedded in the PCL support, leaving exposed to the outside only the surface layer (Figure 1D).

The entire printing and incorporation process enabled assembling sheets containing 24 3DEPs in approximatively 3 hours. Then, after immersion in water for 10 min for washing and drying, strips of adhesive tape were placed onto the top of the 3D printed devices to delimitate the active surface of the WE and at the same time to protect electrical connections from contact with liquid samples (Figure 1E).

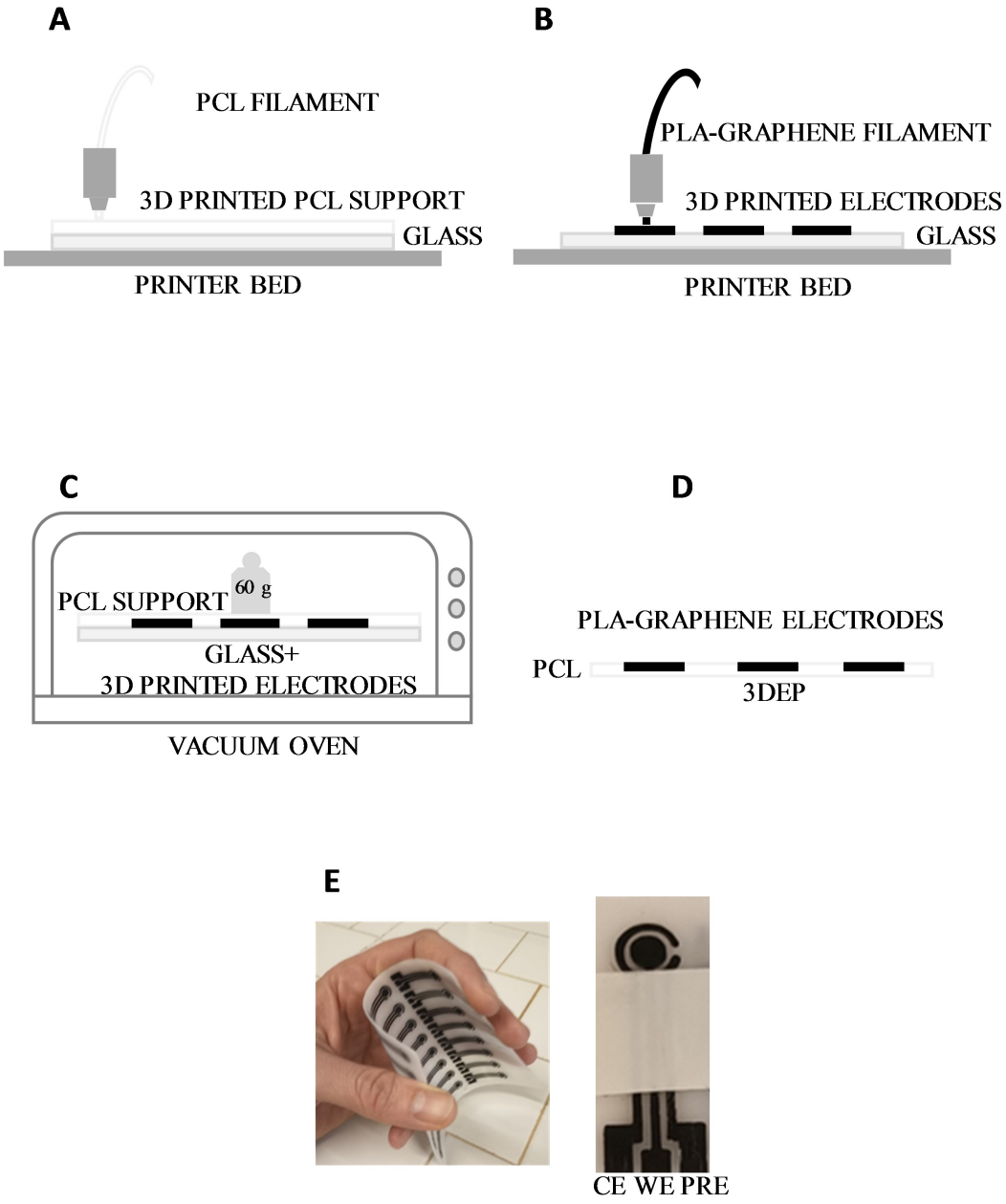

FIGURE 1 (A, B, C, D) Schematic view of the fabrication process. (E) Pictures of 3D printed flexible electrochemical platforms (3DEPs).

2.3 | Activation of 3D printed electrodes

Activation of 3D printed electrodes consisted of two steps. In the first step, electrochemical platforms were immersed in a 0.5 M NaOH aqueous solution and sonicated for 60 min. This step was intended to cause efficient chemical etching of PLA wrapping around the conductive graphene and of PCL residues by hydrolysis, in order to expose, as much as possible, the conductive graphene present on printed electrode surfaces. The second step consisted of a single cycle of electrochemical activation in 0.5 M NaOH aqueous solution carried out by firstly applying an anodic potential of +1.4 V *vs.* Ag/AgCl for 200 s and then a cathodic potential of −1.0 V *vs.* Ag/AgCl for 200 s, according to the procedure described elsewhere [45, 46]. Finally, 3DEPs were rinsed with deionized water and dried for at least 20 min before use.

2.4 | Electrochemical measurements

3DEPs were intended for performing measurements on small volume of samples (50 μL) directly applied to the cell, which was placed in horizontal position onto a planar surface (drop mode). The electrochemical behavior of electrodes was studied using a 0.1 M KCl solution

containing 1 mM of $K_4[Fe(CN)_6]$. This analyte was chosen as redox prototype in view of its well-known reversible electrochemical behavior. Cyclic voltammetric experiments were run in the potential window from −0.2 V to +0.7 V *vs.* Ag/AgCl at different scan rates.

Experiments using HBA and Ty were carried out to evaluate the effect of ultrasonic cleaning and electrochemical activation, after electrode passivation using cyclic voltammetry in the potential window from −0.2 to +1.2 V and +0.4 to +1.5 V *vs.* Ag/AgCl, respectively, at a scan rate of 50 mV/s.

The electrochemical behavior of erioglaucine on 3DPEs was studied using cyclic voltammetry in the potential window from −0.2 to +1.0 V at a scan rate of 50 mV/s using the internal PRE electrode.

Differential pulse voltammetry was used for the quantitative determination of the dye using the following parameters: potential range, +0.4–+1.0 V; pulse amplitude, 0.10 V; pulse width, 0.15 s; pulse duration, 0.15 s; sample period, 0.02 s; pulse period, 0.6 s; scan rate, 6.7 mVs^{-1}.

Commercial solutions of erioglaucine used for homemade food coloring were purchased from local supermarkets. Before analysis, they were simply diluted 1:200 with the sodium phosphate solution (0.1 M; pH = 7).

3 | RESULTS AND DISCUSSION

3.1 | Activation and characterization of 3D printed electrodes

The electrochemical behavior of 3DEPs following different electrode pre-treatments was evaluated by recording cyclic voltammograms for 1 mM hexacyanoferrate(II) solution in 0.1 M KCl supporting electrolyte. Firstly, experiments were conducted using an external Ag/AgCl reference electrode in order to have a stable reference potential.

Cyclic voltammetric experiments were firstly performed at electrodes as printed (AP) and electrochemically activated (EA) using the procedure described in the experimental section. Then a sonication pre-treatment in NaOH aqueous bath (0.5 M) for 60 min was carried out and electrodes sonicated (SA) or electrochemically activated after sonication (SA + EA) were tested. In Figure 2A results achieved using different activation procedures are reported.

It is clearly evident that the response of PLA-graphene electrodes as printed (AP) was very poor [26, 32, 47, 48] and their electrochemical activity limited by the scarce conductivity of the filament used without treatments, while both sonication and electrochemical activation, even if performed separately, led to better electrochemical responses. Furthermore, when sonication and electrochemical activation were applied in sequence, the resulting electrochemical signal definitely increased in current magnitude and improved in shape.

The effect of different pre-treatments on the electrode surface was also evaluated by SEM characterization (Figure 2B) revealing that the morphology of untreated and treated electrodes considerably changed as a result of the removal of part of PLA from the electrode surface causing a dramatic increase of the graphene exposed to the outside. On the basis of the good results obtained applying a combination of sonication and electrochemical activation, the effect of different sonication times on electrochemical performance was explored (Figure 3A). In all cases, the same electrochemical activation procedure, described in the experimental section, was performed after sonication. The increase of sonication time from 15 to 60 min improved the intensity of the electrochemical signal and reduced peak-to-peak separation (ΔE_p). At about 60 min a plateau was reached while a negligible improvement of the electrochemical signal was observed when a longer sonication time was applied. Thus, sonication for 60 min resulted the best compromise to achieve good electrochemical performance in a reasonable time. As expected, voltammetric profiles recorded using the printed pseudo-reference electrode were characterized by a shift of the potential during measurements. This behavior was observed both in 3DPEs subjected only to sonication (SA) and in those in which electrochemical activation was also carried out (SA + EA), this last shown in Figure 3B.

3.2 | Electrochemical performance of 3DEPs

After these preliminary experiments, intra and inter repeatability of electrodes was checked. In particular, good inter electrodes repeatability was obtained with a RSD of 7.3 and 8.2 % for peak currents (both i_{pa} and i_{pc}) and peak-to-peak separation potential (ΔE_p) respectively, on 30 3D printed electrochemical platforms chosen randomly from 15 different batches assembled in different days.

The electrochemically active area of the working electrode after the optimization of the pre-treatment was estimated using the Randel-Ševčík equation (1) applied to cyclic voltammograms of the redox probe $K_4[Fe(CN)_6]$.

$$i_p = 0.4463\ nFAC\sqrt{\frac{nF\nu D}{RT}} \quad (1)$$

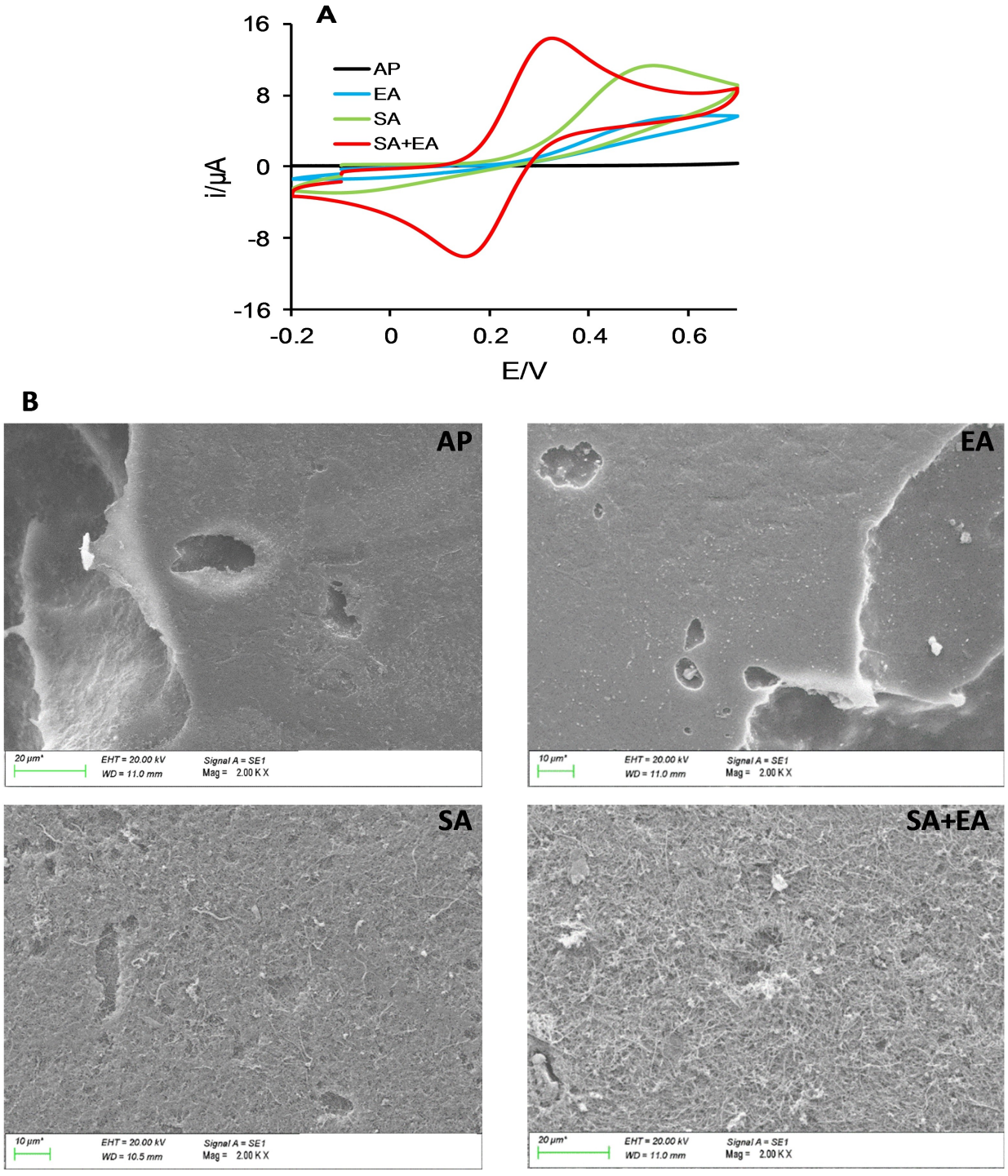

FIGURE 2 (A) Cyclic voltammograms recorded in 0.1 M KCl solution containing 1 mM of $K_4[Fe(CN)_6]$ using 3DEP: as-printed (AP), sonicated (SA), electroactivated (EA), electroactivated after sonication (SA + EA). SA: 60 min in 0.5 M NaOH. EA: +1.4 V (200 s) and −1.0 V (200 s) in 0.5 M NaOH. Scan rate: 50 mV s^{-1}. Reference electrode: Ag/AgCl. (B) SEM images (2000x) of the working electrode surface before (AP) and after different pre-treatments (SA, EA, SA + EA).

where i_p is the peak current, n is the number of electrons transferred ($n=1$), F is the Faraday constant ($F=$ 96485 C mol^{-1}), A is the electrode area (cm^2), C is the concentration of the redox probe (mol cm^{-3}), v is the scan rate (Vs^{-1}), D is the diffusion coefficient ($D=$ $6.8x10^{-6}$ cm^2s^{-1} for $K_4[Fe(CN)_6]$ in 0.1 M KCl supporting electrolyte [49]), R is the gas constant ($R=8.314$ J K^{-1} mol^{-1}) and T is the temperature ($T=298$ K).

The active surface area of the WE estimated by Eq. 1 resulted to be 9.7 ± 0.6 mm^2, slightly lower than the geometric area of 12.6 mm^2 (diameter 4 mm). As a matter of fact, the active surface strongly depends on the loading

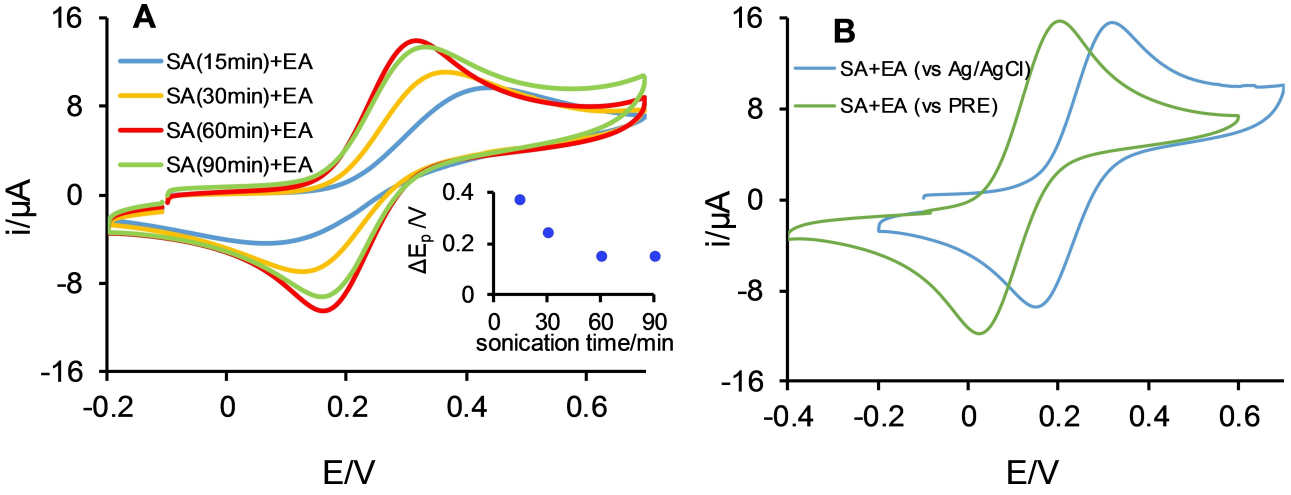

FIGURE 3 Cyclic voltammograms recorded in 0.1 M KCl solution containing 1 mM of $K_4[Fe(CN)_6]$ using 3DEP: (A) sonicated (SA) for different time (15, 30, 60, 90 min) and electroactivated (EA). Reference electrode: Ag/AgCl. SA: in 0.5 M NaOH. EA: +1.4 V (200 s) and −1.0 V (200 s) in 0.5 M NaOH. Scan rate: 50 mV s^{-1}. (B) sonicated (SA) for 60 min and electroactivated (EA), tested *vs.* Ag/AgCl or 3D printed pseudo-reference electrode (PRE). Inset: peak potential difference (ΔE_P) measured for different sonication times.

of graphene of the filament but it is also related to the roughness of the electrode surface. Taking into account only the loading-effect, it being estimated from the content of graphene in the PLA/graphene filament around 8% [50, 51], the active area should result about 1 mm^2. However, the pre-treatment and in particular the sonication step, caused an increase of the superficial roughness with a consequent rise of the active surface. In fact, from SEM images (Figure 2B), it is possible to observe a dramatic increase in surface roughness after pre-treatment thus confirming the effectiveness of the procedure developed which ensured effective removal of non-conductive PLA and the consequent exposition of further conductive particles at the surface of the electrode thus resulting in a remarkable enhancement of electron transfer.

The peak-to-peak separation potential (ΔE_p) measured at a scan rate of 50 mV/s at the most efficient condition of pre-treatment was 150 ± 12 mV. This result, together with the anodic-to-cathodic current ratio quite close to 1 (i_{pa} /i_{pc} = 0.95), pointed out the reversibility of the electrochemical process and the good electrochemical properties of the electrode. Despite the use of a simple method of pre-treatment, totally free from the use of solvents, mechanical polishing and heating, the peak-to-peak separation value (ΔE_p) achieved is at the same level or even better than those reported using other procedures [33, 42, 45, 46, 52, 53].

Moreover, as shown in Figures 4A and 4B, cyclic voltammograms recorded for 1 mM potassium hexacyanoferrate(II) solutions in 0.1 M KCl at scan rates from 5 to 200 mV s^{-1} led to a linear increase of the peak current with the square root of the scan rate. This linear dependence pointed out that the behavior of the tested system (3DEP and redox probe) complied with that expected for diffusion-controlled processes. At the same time, cyclic voltammograms for increasing concentration of potassium hexacyanoferrate(II) solutions in 0.1 M KCl led to a linear increase of the peak current (Figures 4C and 4D) with RSD values ranging from 1.6 and 2.4%.

The standard heterogeneous electron-transfer (HET) rate constant k^0 is a key element to be extracted from electrochemical investigations and gives information about the electron transfer rate between an electroactive species and the electrode surface. It was calculated with the aim of evaluating how the electrode material determines the overall rate of the electrochemical reaction, in the hypothesis that the electrochemically active surface is just that consisting of graphene really uncovered by the non-conductive polymer.

The constant (k^0) was determined using Equation (2) [32, 54, 55], where D is the diffusion coefficient, α is the value of transfer coefficient (assumed to be 0.5), n is the number of electrons involved in the electrochemical process, F is the Faraday constant, R is the gas constant and T is the temperature.

$$k^0 = \left[2.18\left(\frac{D\alpha nFv}{RT}\right)^{1/2}\right] exp\left[-\left(\frac{\alpha^2 nF}{RT}\right)\Delta E_p\right] \quad (2)$$

A k^0 average value of $1.24\times10^{-3} \pm 0.25\times10^{-4}$ cm s^{-1} was calculated for treated electrodes (SA-EA). Similar results were obtained in previous works exploiting composites of PLA with either carbon-black [30, 42] or graphene [47, 53] activated resorting to different treatments, thus demonstrating the success of the proposed

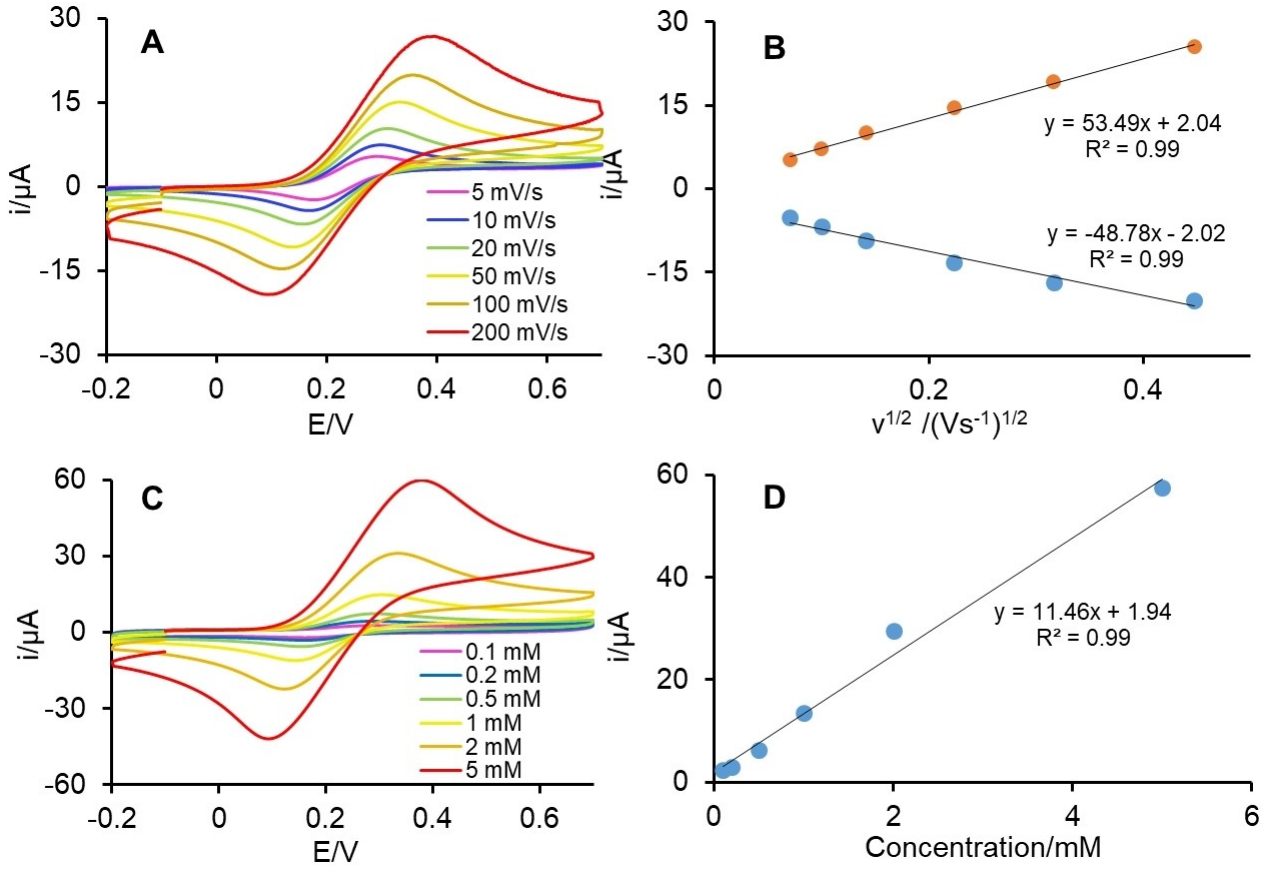

FIGURE 4 (A) Cyclic voltammograms recorded at 3DEP (SA + EA) in 0.1 M KCl solutions containing 1 mM $K_4[Fe(CN)_6]$ at different scan rates (5-200 mV s^{-1}) and (B) correlation between current of anodic (red) and cathodic (blue) peaks and scan rate square root. (C) Cyclic voltammograms recorded for 3DEP (SA + EA) at a scan rate of 50 mV s^{-1} in 0.1 M KCl solution containing increasing concentration of $K_4[Fe(CN)_6]$ (0.1-5 mM) and (D) correlation between anodic peak current and concentration. Reference electrode: Ag/AgCl. SA: 60 min in 0.5 M NaOH. EA: +1.4 V (200 s) and −1.0 V (200 s) in 0.5 M NaOH.

procedure which promoted the efficient hydrolysis of PLA exposing the graphene structures.

Finally, in order to evaluate the elastic behavior of the 3DEPs, their electrochemical performance were tested after 5 bending cycles (5 times at 120°). CV profiles were then compared with those obtained prior to bending tests and no significant differences were observed.

Therefore, it was possible to conclude that the structure of the electrodes after bending caused no alteration able to affect the electrochemical results.

3.3 | Effect of ultrasonic cleaning and electrochemical activation on electrode restoration

Finally, exploiting the effect of the optimized treatment in basic environment, which allows etching of a very thin layer of material at the electrode surface, the restoration of 3DEPs after passivation was verified. In fact, it is well known that during the electrooxidation of some chemical species, such as phenolic compounds, a noticeable decrease in the current is observed due to the electropolymerization of a passivating film on the electrode surface [56–58]. To this aim, replicate cyclic voltammetric scans in the potential window from −0.2 V to +1.2 V *vs.* Ag/AgCl, were run in order to polymerize water soluble HBA onto the working electrode surface. As shown in Figure 5A, the first potential cycle shows an irreversible wave at about 0.7 V related to to the formation of the cation-radical intermediate [59]. A significant decrease of the peak current could be observed during continuous potential cycling, thus confirming that the electrode underwent a gradual passivation due to electropolymerization of phenolic radicals and consequent formation of a polymeric film onto the electrode surface.

In order to restore the functionality of the working electrode, a pre-treatment consisting of sonication in 0.5 M NaOH solution, for 2 min instead of 60 min, followed by electrochemical activation was carried out. Then, the procedure for HBA polymerization was

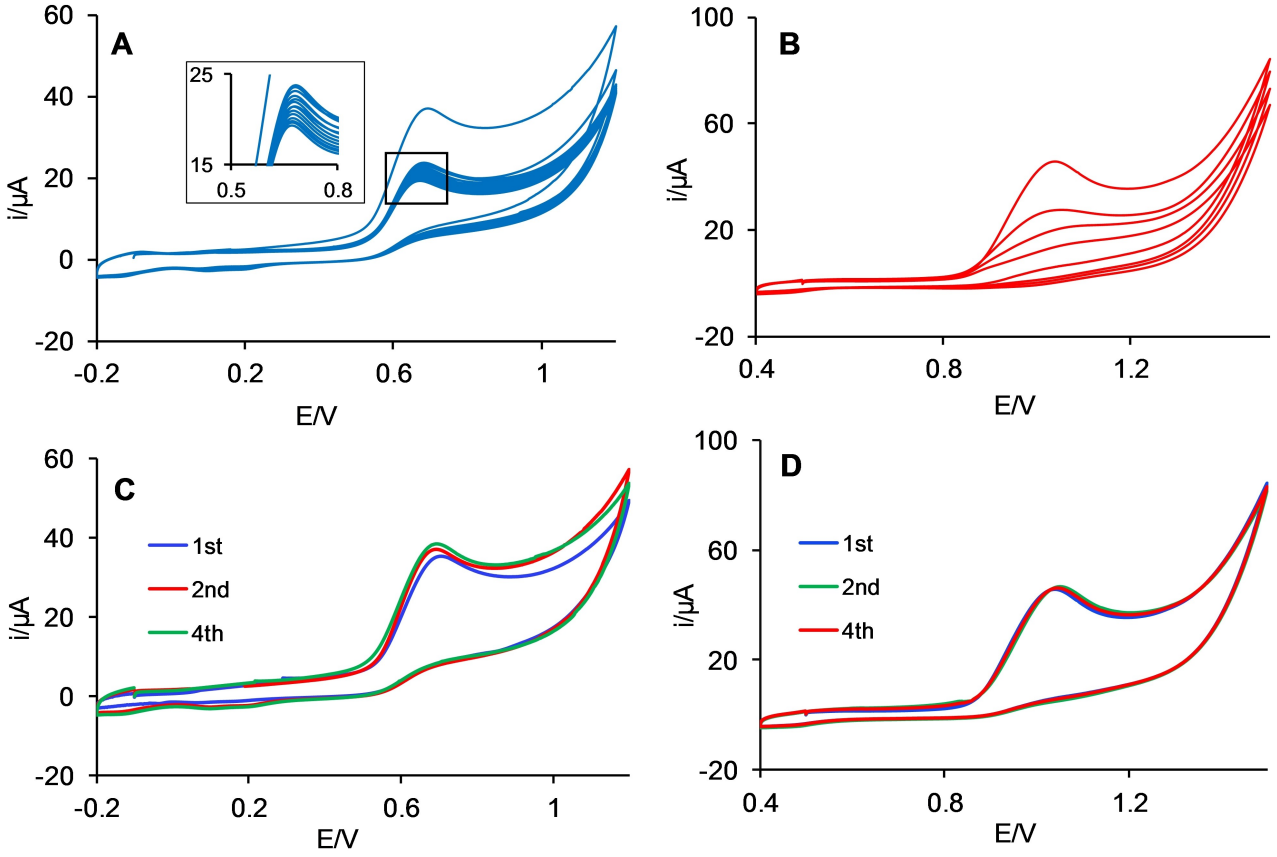

FIGURE 5 (A) Repeated cyclic voltammatric scans recorded at 3DEP (SA + EA) for (A) 2.5×10^{-3} mol L^{-1} of HBA in 0.1 M KCl and (B) 1×10^{-3} mol L^{-1} of Ty in 0.1 M KCl + H_2SO_4. Exemplificative first scans of each of the four series of repetitive voltammetries performed at new 3DEP (SA + EA), 1st, and after the restoring procedure, 2nd-4th for (C) HBA and (D) Ty. Scan rate of 50 mV s^{-1}. Reference electrode: Ag/AgCl. SA: 60 min in 0.5 M NaOH. EA: +1.4 V (200 s) and −1.0 V (200 s) in 0.5 M NaOH. Sonication time for restoring was reduced to 2 min.

repeated. As it can be observed in Figure 5C, the oxidation peak corresponding to the first cycle of the scans returned to be comparable to that initially recorded with the new printed and treated 3DEP. This operation was repeated four times obtaining similar results in terms of peak potentials and currents after each cleaning cycles. Finally, a cyclic voltammetric scan was recorded for comparison purposes for a 0.1 M KCl solution containing 1 mM of the redox probe $K_4[Fe(CN)_6]$ after applying an additional cleaning treatment conducted in the same way as that described previously. The voltammogram recorded indicated that the treatment was effective in restoring the activity of the working electrode removing contamination from its surface by etching the overlayer, thus making 3DEPs completely cleanable and reusable.

A similar experiment was run for 1 mM of Ty, a different phenolic compound, which was dissolved in an acidic media consisting of 0.01 M H_2SO_4 + 0.1 M KCl [61].

Also in this case, after performing consecutive cyclic voltammetric scans in the potential window from 0.4 V to +1.5 V *vs.* Ag/AgCl, a significant decrease of the peak current could be observed during cycling due to the passivation of the working electrode surface (Figure 5B).

The same pre-treatment, consisting of sonication in 0.5 M NaOH solution, for 2 min followed by electrochemical activation was able to restore the functionality of the working electrode. In fact, as it can be observed in Figure 5D, the oxidation peak corresponding to the first cycle of the scans returned to be comparable with that initially recorded with the new printed and treated 3DEP. This operation was repeated four times obtaining similar results in terms of peak potentials and currents after each cleaning cycles.

3.4 | Voltammetric study of erioglaucine and analysis of the real sample

Voltammetric investigations of erioglaucine, a triphenylmethane blue food dye, were first carried to evaluate its

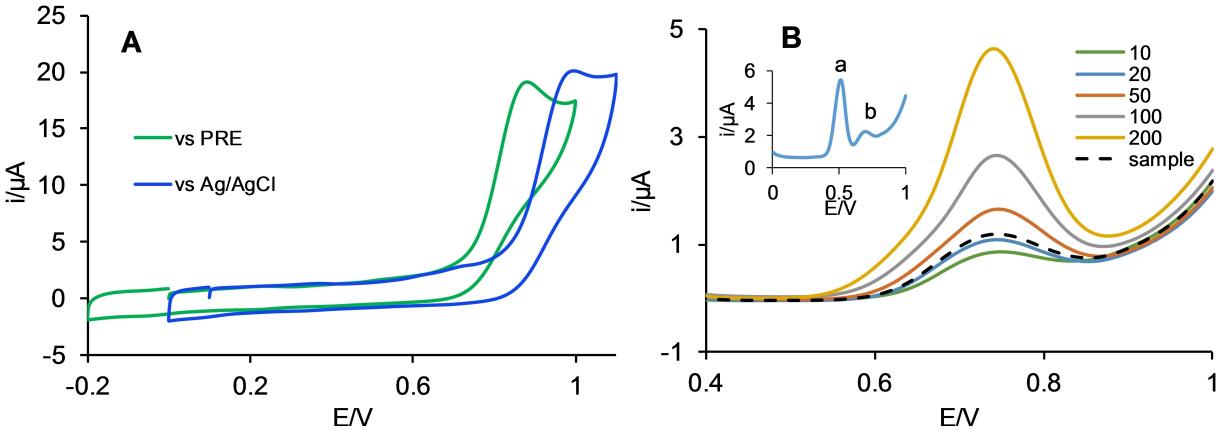

FIGURE 6 (A) Cyclic voltammatric scans recorded at 3DEP (SA + EA) *vs.* Ag/AgCl or *vs.* PRE for 0.5×10^{-3} mol L^{-1} of erioglaucine in 0.1 M phosphate buffer (pH 7). Scan rate 50 mVs^{-1}. (B) Differential pulse voltammograms recorded at 3DEP *vs.* PRE for erioglaucine solutions at the reported concentrations (10-200 μM) in 0.1 M phosphate buffer (pH 7) as supporting electrolyte, together with the DPV voltammogram of a diluted (1 : 200) real sample (−-−). Inset: DPV voltammogram recorded at 3DEP for a synthetic sample containing 20 μM of sunset yellow (a), and 20 μM of erioglaucine (b).

redox behavior using 3DEPs. Measurements were carried out in 0.1 M phosphate solutions at pH 7.0 [62] for a 500 μM solutions of the dye. To better evaluate potentialities of 3DEPs for real applications, these measurements were performed using the internal 3D printed pseudo-reference electrode. From a comparison carried out under the same conditions using an external Ag/AgCl reference electrode, a displacement of the peak potential equal to about 100 mV was observed.

As shown in Figure 6A the blue dye underwent an oxidation process characterized by a peak potential (at about 0.9 V) without causing fouling phenomena at the electrode surface during multiple voltammetric scans.

In order to improve the sensitivity, the determination of the dye was performed by resorting to differential pulse voltammetry (DPV). The measurement parameters, reported in the experimenntal section, were optimized using a solution of erioglaucine 50 μM in 0.1 M aqueous phosphate buffer at pH = 7. At the same time, repeatability intra and inter-device was estimated by running ten consecutive voltammetric scans at the same device or by carrying out DPV tests of the same solution at 5 different 3DEPs. The relative standard deviation (RSD) of peak height values was found to be 6.4 and 7.8% indicating a good repeatability of these measurements. The optimized parameters were subsequently adopted to analyze erioglaucine solutions at increasing concentrations between 10 and 200 μM. As shown in Figure 6B, DPV measurements, performed using optimized conditions, generated well-defined anodic peaks whose height was linearly dependent on the analyte concentration. Then, the calibration curve was calculated on the basis of anodic peak heights and turned out to be $y(\mu A) = 0.0185\ C(\mu M) + 0.277$ with $R^2 = 0.99$. The limit of detection, calculated as $3\sigma/S$ (where σ is the standard deviation calculated on the background noise and S is the sensitivity determined by the calibration curve) was found to be 1.8 μM.

Finally, in order to test the selectivity of the method, experiments were performed by analyzing a mixture containing erioglaucine and Sunset Yellow, another azo-dye frequently used in food.

It is important to note that in order to prevent fouling phenomena, potentially occurring at the electrode when Sunset Yellow was analysed, this last containing a phenolic moiety, a cleaning step was carried out before each DPV experiment.

Quantification of the dye in a commercial solution of the blue food dye was performed by profiting of calibration plots previously constructed by DPV measurements. In particular, a concentration of erioglaucine of approximately 5.1 mM was determined. Similar results were obtained by performing spectrophotometric measurements.

4 | CONCLUSIONS

The innovative proposed approach enables the rapid assembling of flexible planar electrochemical platforms exploiting hot and vacuum-assisted incorporation of 3D printed conductive PLA/graphene tracks within a flexible PCL support without resorting to a dual extruder printer.

The obtained 3DEPs are characterized by a perfectly smooth surface with no discontinuity, irregularities or parts in relief since during both 3D printing and

incorporation steps, materials were pressed against the glass bed [60].

Moreover, they can be produced using reduced quantity of material (ca. 30 and 250 mg of PLA/graphene and PCL, respectively, for a single 3DEP) at very low-cost (ca. 0.04 € for a single 3DEP) mainly due to the cost of the conductive filament used in this study (ca. 70%).

In addition, the use of a new sustainable and rapid pre-treatment procedure, requiring no operator skills and consisting of sequential sonication and electrochemical activation steps, not only allows to increase dramatically the electrode activity, allowing good HET rate and reproducible results to be achieved, but also to clean and regenerate the electrode surface for their multiple reuse.

ACKNOWLEDGMENTS

We thank prof. Lorenzo Fedrizzi and dr. Alfredo Rondinella, of the Polytechnic Department of Engineering and Architecture, of the University of Udine, for SEM measurements.

DATA AVAILABILITY STATEMENT

Research data are not shared.

ORCID

Rossella Svigelj http://orcid.org/0000-0002-5763-0551
Nicolò Dossi http://orcid.org/0000-0002-2136-3260

REFERENCES

1. A. M. E. Arefin, N. R. Khatri, N. Kulkarni, P. F. Egan, *Polymer* **2021**, *13*, 1.
2. H. Tetsuka, S. R. Shin, *J. Mater. Chem. B* **2020**, *8*, 2930.
3. H. K. Balakrishnan, F. Badar, E. H. Doeven, J. I. Novak, A. Merenda, L. F. Dumée, J. Loy, R. M. Guijt, *Anal. Chem.* **2021**, *93*, 350.
4. L. Wang, M. Pumera, *TrAC Trends Anal. Chem.* **2021**, *135*, 116151.
5. A. Ambrosi, A. Bonanni, *Microchim. Acta* **2021**, *188*, 265.
6. M. Belka, T. Bączek, *TrAC Trends Anal. Chem.* **2021**, *142*, 116322.
7. S. Hermanová, M. Pumera, *Bioprinting* **2022**, *26*, e00198.
8. B. Almuallim, W. S. W. Harun, I. J. Al Rikabi, H. A. Mohammed, *J. Mater. Sci.* **2022**, *57*, 3993.
9. C. Amni Marwan, S. Aprilia, E. Indarti, *IOP Conf. Ser. Earth Environ. Sci.* **2021**, *926*, 012080.
10. G. Faura, C. Grazioli, N. Dossi, R. Svigelj, R. Toniolo, G. Bontempelli, *Microchem. J.* **2021**, *170*, 106690.
11. C. Kalinke, P. R. de Oliveira, N. V. Neumsteir, B. F. Henriques, G. de Oliveira Aparecido, H. C. Loureiro, B. C. Janegitz, J. A. Bonacin, *Anal. Chim. Acta* **2022**, *1191*, 339228.
12. G. Stano, A. Di Nisio, A. M. Lanzolla, M. Ragolia, G. Percoco, *Int. J. Adv. Manuf. Technol.* **2020** *111*, 2971.
13. M. J. Whittingham, R. D. Crapnell, E. J. Rothwell, N. J. Hurst, C. E. Banks, *Talanta Open* **2021**, *4*, 100051.
14. M. H. Omar, K. A. Razak, M. N. Ab Wahab, H. H. Hamzah, *RSC Adv.* **2021**, *11*, 16557.
15. K. Ragazou, R. Lougkovois, V. Katseli, C. Kokkinos, *Sensors* **2021**, *21*, 4753.
16. L. Wang, M. Pumera, *Microchim. Acta.* **2021**, *18*, 81.
17. B. Hüner, N. Demir, M. F. Kaya, *Int. J. Hydrogen Energy* **2022**, *47*, 12136.
18. V. Katic, P. L. Dos Santos, M. F. Dos Santos, B. M. Pires, H. C. Loureiro, A. P. Lima, J. C. M. Queiroz, R. Landers, R. A. A. Muñoz, J. A. Bonacin, *ACS Appl. Mater. Interfaces* **2019**, *11*, 35068.
19. N. Rohaizad, C. C. Mayorga-Martinez, F. Novotný, R. D. Webster, M. Pumera, *Electrochem. Commun.* **2019**, *103*, 104.
20. K. P. A. Kumar, K. Ghosh, O. Alduhaish, M. Pumera, *Electrochem. Commun.* **2020**, *120*, 106827.
21. J. S. Stefano, L. R. Guterres e Silva, R. G. Rocha, L. C. Brazaca, E. M. Richter, R. A. Abarza Muñoz, B. C. Janegitz, *Anal. Chim. Acta* **2021**, *1191*, 339372.
22. R. G. Rocha, R. M. Cardoso, P. J. Zambiazi, S. V. F. Castro, T. V. B. Ferraz, G. de O. Aparecido, J. A. Bonacin, R. A. A. Munoz, E. M. Richter, *Anal. Chim. Acta* **2020**, *1132*, 1–9.
23. J. S. Stefano, C. Kalinke, R. G. da Rocha, D. P. Rocha, V. A. O. P. da Silva, J. A. Bonacin, L. Angnes, E. M. Richter, B. C. Janegitz, R. A. A. Muñoz, *Anal. Chem.* **2022**, *94*, 6417.
24. A. L. Silva, G. M. da S. Salvador, S. V. F. Castro, N. M. F. Carvalho, R. A. A. Munoz, *Front. Chem.* **2021**, *9*, 684256.
25. D. M. Wirth, M. J. Sheaff, J. V. Waldman, M. P. Symcox, H. D. Whitehead, J. D. Sharp, J. R. Doerfler, A. A. Lamar, G. Leblanc, *Anal. Chem.* **2019**, *91*, 5553.
26. M. P. Browne, F. Novotný, Z. Sofer, M. Pumera, *ACS Appl. Mater. Interfaces* **2018**, *10*, 40294.
27. J. E. Contreras-Naranjo, V. H. Perez-Gonzalez, M. A. Mata-Gómez, O. Aguilar, *Electrochem. Commun.* **2021**, *130*, 107098.
28. M. A. Ragolia, A. M. L. Lanzolla, G. Percoco, G. Stano, Attilio Di Nisio, *Sensors* **2021**, *21*, 6324.
29. R. D. Crapnell, E. Bernalte, A. G.-M. Ferrari, M. J. Whittingham, R. J. Williams, N. J. Hurst, C. E. Banks, *ACS Meas. Sci. Au* **2021**, *2*, 167.
30. G. D. O'Neil, S. Ahmed, K. Halloran, J. N. Janusz, A. Rodriguez, I. M. Rodriguez, *Electrochem. Commun.* **2019**, *99*, 56.
31. S. M. Sibug-Torres, L. P. Go, V. C. G. Castillo, J. L. R. Pauco, E. P. Enriquez, *Anal. Chim. Acta* **2021**, *1160*, 338430.
32. C. Kalinke, N. V. Neumsteir, G. O. Aparecido, T. V. B. Ferraz, P. L. Dos Santos, B. C. Janegitz, J. A. Bonacin, *Analyst* **2020**, *145*, 1207.
33. D. P. Rocha, R. G. Rocha, S. V. F. Castro, M. A. G. Trindade, R. A. A. Munoz, E. M. Richter, L. Angnes, P *Electrochem. Sci. Adv.* **2021**, *2*, e2100136.
34. F. Novotný, V. Urbanová, J. Plutnar, M. Pumera, *ACS Appl. Mater. Interfaces.* **2019**, *11*, 35371.
35. R. Gusmão, M. P. Browne, Z. Sofer, M. Pumera, *Electrochem. Commun.* **2019**, *102*, 83. https://doi.org/10.1016/j.elecom.2019.04.004.
36. C. L. Manzanares Palenzuela, F. Novotný, P. Krupička, Z. Sofer, M. Pumera, *Anal. Chem.* **2018**, *90*, 5753.

37. R. M. Cardoso, P. R. L. Silva, A. P. Lima, D. P. Rocha, T. C. Oliveira, T. M. do Prado, E. L. Fava, O. Fatibello-Filho, E. M. Richter, R. A. A. Muñoz, *Sens. Actuators B* **2020**, *307*, 127621.
38. G. Martins, J. L. Gogola, L. H. Budni, B. C. Janegitz, L. H. Marcolino-Junior, M. F. Bergamini, *Anal. Chim. Acta* **2021**, *1147*, 30.
39. I. Fortelny, A. Ujcic, L. Fambri, M. Slouf, *Front. Mater.* **2019**, *6*, 1.
40. M. Schneider, N. Fritzsche, A. Puciul-Malinowska, A. Baliś, A. Mostafa, I. Bald, S. Zapotoczny, A. Taubert, *Polymer* **2020**, *12*, 1711.
41. D. Gupta, A. K. Singh, N. Kar, A. Dravid, J. Bellare, *Mater. Sci. Eng. C.* **2019**, *98*, 602.
42. A. Koterwa, I. Kaczmarzyk, S. Mania, M. Cieslik, R. Tylingo, T. Ossowski, R. Bogdanowicz, P. Niedziałkowski, J. Ryl, *Appl. Surf. Sci.* **2022**, *574*, 151587.
43. Q. Yuan, Y. Liu, C. Ye, H. Sun, D. Dai, Q. Wei, G. Lai, T. Wu, A. Yu, L. Fu, K. W. A. Chee, C. Te Lin, *Biosens. Bioelectron.* **2018**, *111*, 117.
44. B. R. Kozub, N. V. Rees, R. G. Compton, *Sens. Actuators B* **2010**, *143*, 539.
45. E. M. Richter, D. P. Rocha, R. M. Cardoso, E. M. Keefe, C. W. Foster, R. A. A. Munoz, C. E. Banks, *Anal. Chem.* **2019**, *91*, 12844.
46. F. M. de Oliveira, E. I. de Melo, R. A. B. da Silva, *Sens. Actuators B* **2022**, *360*, 131650.
47. C. Kalinke, N. Neumsteir, P. R. de Oliveira, B. Campos Janegitz, J. A. Bonacin, *Anal. Chim. Acta* **2021**, *1142*, 135e142.
48. V. A. O. P. Silva a, W. S. Fernandes-Junior, D. P. Rocha, J. S. Stefano, R. A. A. Munoz, J. A. Bonacin, B. C. Janegitz, *Biosens. Bioelectron.* **2020**, *170*, 112684.
49. S. J. Konopka, B. McDuffie, *Anal. Chem.* **1970**, *42*, 1741.
50. C. Y. Foo, H. N. Lim, M. A. Mahdi, M. H. Wahid, N. M. Huang, *Sci. Rep.* **2018**, *8*, 7399.
51. C. W. Foster, M. P. Down, Y. Zhang, X. Ji, S. J. Rowley-Neale, G. C. Smith, P. J. Kelly, C. E. Banks, *Sci. Rep.* **2017**, *7*, 1.
52. J. F. S. Pereira, R. G. Rocha, S. V. F. Castro, A. F. João, P. H. S. Borges, D. P. Rocha, A. de Siervo, E. M. Richter, E. Nossol, R. V. Gelamo, R. A. A. Muñoz, *Sens. Actuators B* **2021**, *347*, 130651.
53. H. A. Silva-Neto, M. Santhiago, L. C. Duarte, W. K. T. Coltro, *Sens. Actuators B* **2021**, *349*, 1.
54. P. L. dos Santos, V. Katic, H. C. Loureiro, M. F. dos Santos, D. P. dos Santos, A. L. B. Formiga, J. A. Bonacin, *Sens. Actuators: B. Chem.* **2019**, *281*, 837.
55. R. J. Klingler, J. K. Kochi, *J. Phys. Chem.* **1981**, *85*, 1741.
56. M. Ferreira, H. Varela, R. M. Torresi, G. Tremiliosi-Filho, *Electrochim. Acta.* **2006**, *52*, 434.
57. N. Belhadj Tahar, A. Savall, *J. Appl. Electrochem.* **2011**, *41*, 983.
58. H. Barich, R. Cánovas, K. De Wael, *J. Electroanal. Chem.* **2022**, *904*, 115878.
59. L. F. Ferreira, L. M. Souza, D. L. Franco, A. C. H. Castro, A. A. Oliveira, J. F. C. Boodts, A. G. Brito-Madurro, J. M. Madurro, *Mater. Chem. and Phys.* **2011**, *129*, 46.
60. H. H. Bin Hamzah, O. Keattch, D. Covill, B. A. Patel, *Sci. Rep.* **2018**, *8*, 1.
61. N. Dossi, R. Toniolo, F. Terzi, N. Sdrigotti, F. Tubaro, G. Bontempelli, *Anal. Chim. Acta* **2018**, *21*, 1040, 74.
62. N. Dossi, R. Toniolo, F. Terzi, C. Grazioli, R. Svigelj, F. Gobbi, G. Bontempelli, *Electroanalysis* **2020**, *32*, 291.

How to cite this article: C. Grazioli, R. Svigelj, N. Dossi, *Electroanalysis* **2023**, *35*, e202300013. https://doi.org/10.1002/elan.202300013

Graphical Abstract

The contents of this page will be used as part of the graphical abstract of html only.
It will not be published as part of main.